Coupling kinetic Monte Carlo and finite element methods to model the strain path sensitivity of the isothermal stress-assisted martensite nucleation in TRIP-assisted steels

Stephen Cluff, Marko Knezevic, Michael P. Miles, David T. Fullwood, Raja K. Mishra, Anil K. Sachdev, Tyson Brown, Eric R. Homer

PII: S0167-6636(20)30735-3

DOI: https://doi.org/10.1016/j.mechmat.2020.103707

Reference: MECMAT 103707

To appear in: Mechanics of Materials

Received date: 19 June 2020 Revised date: 23 November 2020 Accepted date: 2 December 2020



Please cite this article as: S. Cluff, M. Knezevic, M.P. Miles et al., Coupling kinetic Monte Carlo and finite element methods to model the strain path sensitivity of the isothermal stress-assisted martensite nucleation in TRIP-assisted steels. *Mechanics of Materials* (2020), doi: https://doi.org/10.1016/j.mechmat.2020.103707.

This is a PDF file of an article that has undergone enhancements after acceptance, such as the addition of a cover page and metadata, and formatting for readability, but it is not yet the definitive version of record. This version will undergo additional copyediting, typesetting and review before it is published in its final form, but we are providing this version to give early visibility of the article. Please note that, during the production process, errors may be discovered which could affect the content, and all legal disclaimers that apply to the journal pertain.

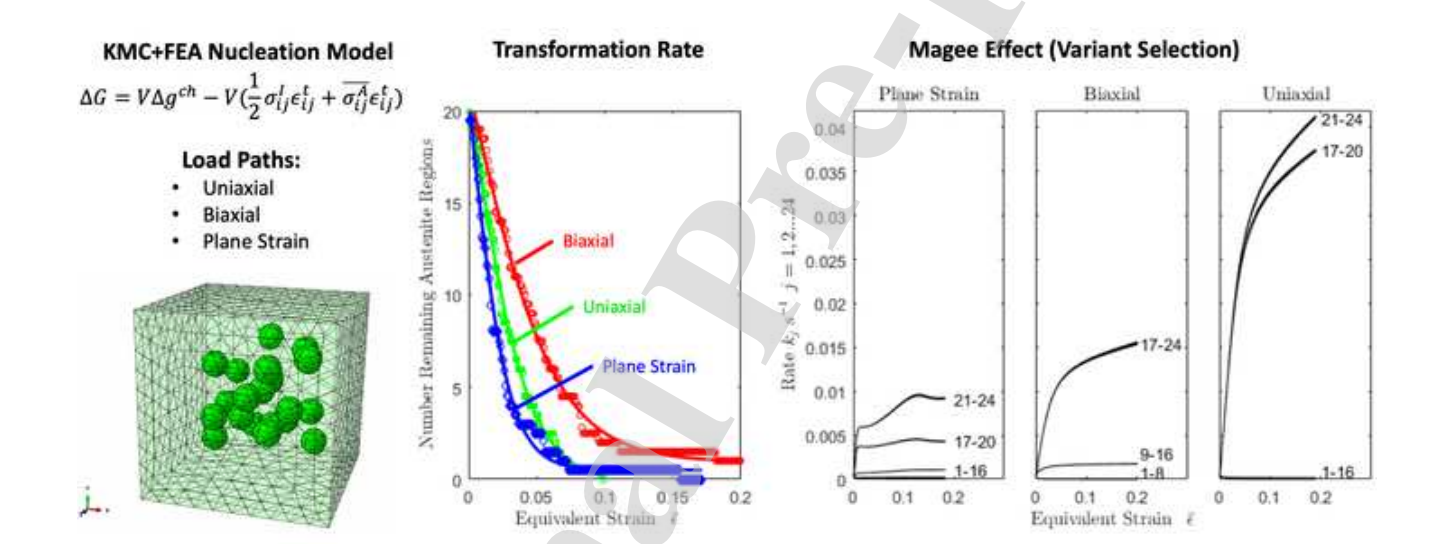
© 2020 Published by Elsevier Ltd.

Highlights

- Model is developed to simulate the kinetics of isothermal stress-assisted martensite nucleation that couples the kinetic Monte Carlo method with the finite element method
- Model is validated against austenite transformation data for a TADP steel alloy for the purpose
 of studying isothermal nucleation kinetics in TRIP-assisted steels generally
- The nucleation kinetics of martensite is shown to be affected by strain path, and the adjacency of nucleation events (kinematic coupling)
- The underlying phenomenon that governs differences of nucleation kinetics is discussed in the context of the Magee effect, both generally and for TRIP-assisted steels
- The plane strain is shown to be the most sensitive to kinematic coupling, while the uniaxial and biaxial strain paths show little sensitivity to kinematic coupling

Graphical Abstract

Click here to access/download;Graphical Abstract;graphical_abstract.png ±



Coupling Kinetic Monte Carlo and Finite Element Methods to Model the Strain Path Sensitivity of the Isothermal Stress-assisted Martensite Nucleation in TRIP-assisted Steels

Stephen Cluff^a, Marko Knezevic^c, Michael P. Miles^b, David T. Fullwood^a, Raja K. Mishra^d, Anil K. Sachdev^d, Tyson Brown^d, Eric R. Homer^{a,*}

^aDepartment of Mechanical Engineering, Brigham Young University, Provo, UT, USA
^bDepartment of Manufacturing Engineering, Brigham Young University, Provo, UT, USA
^cDepartment of Mechanical Engineering, University of New Hampshire, Durham, NH 03824, USA
^dGeneral Motors Global Research & Development, Warren, MI 48090, USA

Abstract

The properties of TRIP-assisted steels are influenced by the transformation of retained austenite into martensite during deformation via the mechanically-induced martensite transformation. In the present work the effect of strain path on isothermal stress-assisted martensite nucleation and variant selection are studied by the coupling of the kinetic Monte Carlo method with the finite element method. This coupled model centers on a thermomechanical model of the martensitic transformation, and the model is tuned and validated against transformation data gathered experimentally for a TRIP-assisted dual phase steel (Ennis et al., Int. J. Plast., 2017, 88, 126.). The effect of the proximity of adjacently transforming regions (kinematic coupling) is also studied as a function of strain path. The model results demonstrate how the rate of martensite nucleation is affected by the strain path (uniaxial tension, biaxial tension, and plane strain) and how the kinematic coupling between adjacent transforming regions is unique to each path. These phenomena are discussed in the context of the Magee effect, which is the relationship between stress state and the suppression/assistance of the nucleation of specific variants of martensite. The implications of martensite nucleation's sensitivity to strain path and kinematic coupling are discussed for TRIP-assisted steels that transform by isothermal stress-assisted nucleation.

Keywords: Martensite; TRIP steel; Phase transformation; Kinetic Monte Carlo; Finite element method

1. Introduction

The martensite transformation is a well-studied crystallographic phenomenon in steels, and the thermomechanics and crystallography of martensite have been well described in the literature (Christian, 1975; Balluffi et al., 2005; Pereloma and Edmonds, 2012). The theoretical body of work on martensite is referred to as the phenomenological theory of martensite crystallography (PTMC), and describes the crystallography of the martensite transformation in detail (Bowles and Mackenzie, 1954; Mackenzie and Bowles, 1954; Wechsler et al., 1953). Many models utilizing the PTMC have been developed to explain, study, and simulate the nucleation and growth of martensite in various steels under varied processing schemes. Such models have contributed to the development of new steels, which continue to emerge with the goal of achieving improved strength and formability (Matlock and Speer, 2009). One such class of steel is the set of advanced high strength steels (AHSS) that are assisted by the transformation-induced plasticity (TRIP) phenomenon (Olson and Azrin, 1978; Olson and Cohen, 1982b). These steels have small amounts of retained austenite which transform into martensite upon loading. For some alloys this transformation happens isothermally under

ite. The current work seeks to investigate the role of strain path on the isothermal stress-assisted nucleation of martensite in TRIP-assisted steels. The goal remains the same, however,

of improving the impact that the TRIP effect has on automotive

the driving force of applied stress (stress-assisted). For others, the transformation is triggered by plasticity within the re-

tained austenite (strain-induced). For both such modes of nucle-

ation, the martensite transformation contributes to plastic flow

when such materials are deformed, resulting in greater harden-

ing rates and improved ductility/formability (Olson and Cohen,

1982b; Seo et al., 2016; Cramer et al., 2018). Steels exhibit-

ing this behavior are identified as TRIP or TRIP-assisted steels,

and are of particular interest to the automotive industry (Mat-

Several studies on the sensitivity of material response to

strain path have emerged for TRIP and TRIP-assisted steels (Yu

lock and Speer, 2009).

Preprint submitted to Computational Materials Science

November 23, 2020

et al., 2006; Perdahcioğlu et al., 2008; Zecevic et al., 2019). Recent studies on quenched and partitioned (Q&P) and TRIP alloys have focused on how the transformation of austenite affects the forming limit diagrams of these steels (Cramer et al., 2018; Gibbs, 2019). Another study investigates the transformation behavior of a TRIP-assisted dual phase steel (TADP) as a function of strain and contrasts the results with another automotive dual phase steel (Ennis et al., 2017). The majority of these works, however, focus on the strain path dependence of the strain-induced nucleation of martensite within retained austen-

^{*}Corresponding author

Email address: eric.homer@byu.edu (Eric R. Homer)

materials by clarifying its dependence on strain path.

1.1. Kinetics of martensite nucleation in steels

Generally, the nucleation and growth of martensite in steel has been described from both continuum-elastic and discretedislocation points of view, as the crystallographic theory of martensite has been sufficiently developed to provide insight into the dislocation structures that form the austenite-martensite boundary (Olson and Cohen, 1982a, 1986). The formation of martensite is considered to be nucleation controlled; a nucleation event is followed by an auto-catalytic growth stage where the austenite-martensite boundary propagates at a high velocity determined by the rate at which the boundary dislocations can move together as a glissile interface. While the growth of martensite appears to be barrierless, the barrier to martensite nucleation is far too great for martensite to nucleate homogeneously. It is understood that the nucleation of martensite is primarily heterogeneous (Pati and Cohen, 1969; Olson and Cohen, 1975b), occurring at sites where dislocation structures or grain boundaries provide sufficient free energy to overcome the large barrier to nucleation.

The nucleation of martensite at viable heterogeneous sites can occur through different means. The spontaneous nucleation of martensite via rapid cooling is often referred to as "athermal" martensite, and the temperature range of its formation is identified by the martensite start and finish temperatures, denoted as M_s and M_f respectively (Olson and Azrin, 1978; Pereloma and Edmonds, 2012). For a given alloy held at a temperature at which some volume fraction of austenite remains stable, the martensite transformation can be triggered by the application of either stress or deformation. These two modes are the so-called stress-assisted and strain-induced modes of martensite nucleation. Stress-assisted nucleation occurs isothermally as applied stress fields provide elastic strain energy needed for existing nucleation sites to overcome the barrier to nucleation (Pati and Cohen, 1969; Olson and Azrin, 1978; Olson and Cohen, 1982b). Strain-induced nucleation occurs as plasticity in the retained austenite creates new nucleation sites via the creation and intersection of ε -martensite shear bands (Olson and Cohen, 1975b; Olson and Azrin, 1978; Olson and Cohen, 1982a, 1986). These two nucleation behaviors dominate distinct ranges between the M_s and M_f temperatures, with the boundary between nucleation modes often denoted as M_s^{σ} . At temperatures below M_s^{σ} , the nucleation behaviors of retained austenite are assumed to be stress-assisted (Olson and Azrin, 1978; Pereloma and Edmonds, 2012). The various TRIP-assisted steels can be categorized by which of these two modes of nucleation occurs. Transformation of austenite that occurs via either of these two nucleation modes is referred to as a mechanically induced martensite transformation (Marketz and Fischer, 1994; Pereloma and Edmonds, 2012; Haidemenopoulos et al., 2014).

The application of stress in the stress-assisted nucleation of martensite at available heterogeneous sites plays a role in the selection of which variants of martensite actually form (commonly referred to as variant selection) (Marketz and Fischer, 1994; Pereloma and Edmonds, 2012). The stress field that arises from transformation interacts with the stress field caused

by applied loads in a way that may reduce or increase the change in free energy caused by the martensite transformation. If the shape change caused by transformation into a given variant of martensite results in a lower stress state, then that variant is said to be assisted by the applied stress. This is known as the Magee effect (Marketz and Fischer, 1994; Pereloma and Edmonds, 2012). Similarly, if the applied stress facilitates the activation of slip systems in the surrounding material so that a transforming martensite particle may transform with less resistance, that variant is said to have been assisted via the Greenwood-Johnson effect (Marketz and Fischer, 1994; Taleb and Sidoroff, 2003). Both of these mechanisms are means by which the stress-assisted martensite transformation can result in a form of variant selection.

1.2. Models of TRIP steels

Built on early work of the thermomechanics of steel alloys (Kaufman and Cohen, 1958; Pati and Cohen, 1969; Olson and Cohen, 1975b, 1982b), substantial work has sought to model the kinetics of martensite nucleation as a function of mechanical deformation in TRIP and TRIP-assisted steels. Several such works describe the effect of strain-induced nucleation of martensite in TRIP steels (Olson and Cohen, 1975b; Olson and Azrin, 1978; Olson and Cohen, 1982b; Stringfellow et al., 1992), proposing that the nucleation of martensite happens most readily at shear-band intersections where dislocation interactions create potent nucleation sites. Studies utilizing this Olson-type model have been extensively applied to various studies of TRIP and TRIP-assisted steels that undergo the strain-induced nucleation of martensite. A review of these works is too large to include in this work. Related studies discuss the nature of the isothermal stress-assisted martensite transformation in other TRIP steels, and describe the kinetics of these transformations in detail (Olson and Cohen, 1982b; Beese and Mohr, 2011; Pereloma and Edmonds, 2012; Mansourinejad and Ketabchi, 2017).

Other successful models have been developed for the simulation of the martensite transformation in TRIP steels that take a continuum-elastic approach to the martensite transformation and are applied in crystal plasticity codes (Marketz and Fischer, 1994; Turteltaub and Suiker, 2006; Tjahjanto et al., 2008). Some of these authors (Turteltaub and Suiker, 2006; Tjahjanto et al., 2008) have created a model that defines the driving force for the transformation of austenite through the use of a dissipation potential. The transformation rate and its conjugate driving force for a given variant are related through a pre-defined kinetic relationship, and the volume fractions of each variant at a material point are homogenized. In these models, the evolution of the volume fraction of martensite is most commonly modeled as a sigmoidal function of the macroscopic strain. Such empirical modeling is not sensitive to strain-path. To relax the issue, scalar variables like the stress triaxiality (Stringfellow et al., 1992; Santacreu et al., 2006; Haidemenopoulos et al., 2014), or the stress triaxiality and the Lode angle parameter (Lebedev and Kosarchuk, 2000; Beese and Mohr, 2011; Mansourinejad and Ketabchi, 2017), have been introduced in other models for

transformation. These models capture the role of microstructural phenomena, such as texture evolution and anisotropy, using a crystal plasticity-based formulation (Zecevic et al., 2019), which is an extension of a previous elasto-plastic self-consistent model (Zecevic et al., 2016).

The computational modeling of steel has grown to incorporate more known aspects of the thermomechanics of the martensite transformation as high performance computational resources have become available. Monte Carlo methods have served as meso-scale modeling techniques to capture the effect of stochastic processes on bulk mechanical behaviors. This approach is well suited for the simulation of systems that evolve through kinetic processes, such as in the nucleation of martensite. Stochastic models have only recently been applied to martensite. Using the kinetic Monte Carlo (KMC) algorithm, Chen and Schuh (Chen and Schuh, 2015) developed a thermodynamic framework to simulate both the forward and reverse martensitic transformations in a single crystal shape-memory alloy. Presently, no such studies have utilized KMC to study the martensite transformation in TRIP-assisted steels.

1.3. Overview

The current work uses the KMC method to simulate the stress-assisted isothermal nucleation of martensite in TRIPassisted steels generally. The effect that different mechanical states have on nucleation behaviors will be examined. Primary attention is given to the effect of strain/load path on nucleation, differentiating nucleation behaviors observed in uniaxial biaxial, and plane strain conditions. These particular strain/load paths are selected because they are the primary ones used to obtain a forming limit curve, which defines a locus of strain ratios above which necking is likely to occur (Keeler and Backhofen, 1964; Goodwin, 1968; Paul, 2013). This approach is of particular interest to the authors, as it applies to the formability of sheet metal, which is a topic of great interest in the current automotive light-weighting effort where advanced high strength steel, including TRIP-assisted steels, is playing an important role. We study the effect that prior transformations have on subsequent transformation as local stress fields develop, referred to in this work as kinematic coupling. To perform this study, aspects of the microstructures of TRIP-assisted steels will be incorporated into a model that couples the KMC method with an FEA solver to deform a theoretical region of a TRIPassisted steel and simulate the martensite transformation and its accompanying change in shape. For validation and comparison, recent studies that examine the transformation of austenite in TRIP-assisted steels are of particular interest.

One such study is the aforementioned paper by Ennis et al. (2017), which observes the transformation of martensite by in-situ X-ray diffraction during the uniaxial deformation of a TADP steel. The TADP microstructure presented by Ennis consists of retained austenite having a "blocky" morphology, dispersed alongside martensite and bainite within a matrix of ferrite. In this steel the stabilization of retained austenite occurs in part during the formation of bainite, in which carbon is rejected from the newly formed bainite into surrounding austenite. Ennis' conclusions regarding this steel include the observation that

no yielding occurs in the retained austenite, or the subsequent mechanically induced martensite, until the transformation of all retained austenite is complete (Ennis et al., 2017). This forms the basis for the subsequent conclusion that the transformation of retained austenite in this steel occurs by the stress-assisted isothermal nucleation of martensite. Ennis provides transformation data that is valuable for the validation of the model presented here.

Also of interest are recent studies on Q&P alloys (Seo et al., 2016; Cramer et al., 2018). Cramer et al. (2018) performed an experimental study in which the transformation of retained austenite to martensite in a Q&P 1180 alloy is specifically expressed as a function of strain path. Cramer et al. generated this data via ex-situ straining through different strain paths (uniaxial, biaxial, and plane strain) and by measuring the fraction of retained austenite transformed through EBSD imaging. This data is used as a comparison to the output of the current work's model, and discussed in later sections. For another Q&P alloy, the study presented by Seo et al. (2016) goes into more detail on the mechanical behavior of the different phases present during deformation. Seo et al. determine that the matrix phase of primary martensite has a lower yield strength than both the retained austenite and mechanically induced martensite. Though Q&P alloys are considered to undergo the strain-induced martensite transformation upon loading (De Moor et al., 2008; Wang and Speer, 2013; Seo et al., 2016), the Q&P materials presented in these studies have various microstructural features in common with the TADP steel studied by Ennis et al. One such similarity is the morphology of the retained austenite, which can also be described as "blocky".

Crystallographic, kinetic, and thermodynamic aspects of the martensite transformation are considered and included as aspects of the current model. The effect of load path is first studied through a so-called virtual transformation model that utilizes the KMC method to study the effects of bulk stress state on martensite nucleation. The influence of kinematic coupling on model behavior is achieved by the full coupling of the KMC algorithm with an FEA solver to observe how interacting stress fields of adjacent transformed regions influence martensite nucleation. The current work shows how a KMC-FEA coupled model that simulates martensite nucleation can reveal aspects of the relationship between the mechanical state of a TRIP-assisted steel and rates at which its retained austenite transforms.

2. Methods

2.1. Model

The current work seeks to simulate aspects of the martensite transformation in TRIP-assisted steels. Some aspects of TADP and Q&P microstructure are used to inform choices of phase morphology and constitutive behavior within the model, and provide context for results. These materials also inform the choice of several assumptions made in determining the nucleation behaviors and crystallography of the martensite transformation.

First, by the results of Ennis et al. (2017) for the TADP steel studied, we assume in the current model the isothermal stressassisted nucleation of martensite. The current model also assumes that no yielding occurs within the retained austenite until all austenite is transformed, following Ennis' results. Second, the morphology of the retained austenite is assumed to be granular, and the morphology of mechanically induced martensite is assumed to be lath martensite. Third, as martensitic transformations occur quickly once they have nucleated, we model only their nucleation, and once this occurs, the entire surrounding austenite region accompanying the nucleus is all considered to have transformed. From these points we (i) assume isothermal martensite nucleation, (ii) treat the martensite nucleation as primarily assisted by elastic stresses according to the Magee effect, (iii) model the microstructure with a discrete number of potential nucleation sites, and (iv) neglect the creation of new sites that might otherwise appear in strain-induced martensite transformation models. We also neglect the Greenwood-Johnson effect, both for simplicity and speed of model operation.

These assumptions provide the framework necessary to formally define the martensite transformation from thermomechanical and crystallographic points of view. The following sections detail these aspects of the theory underlying the model. Following these, the details of the KMC algorithm are described.

2.1.1. Thermomechanics of the martensite transformation

The nucleation behavior of martensite is a function of both thermal and mechanical variables. As this model seeks to couple nucleation behaviors with the material's mechanical state, the free energy change ΔG of the transformation from austenite to martensite must be defined by a suitable thermodynamic potential. This is done using the Gibbs free energy as a measure of the model's energy state.

A general expression for the Gibbs free energy change of a nucleating martensite particle in the shape of an oblate spheroid is given by Kaufman and Cohen (1958), and is later restated by Olson and Cohen (1975a); Pereloma and Edmonds (2012) in the following form

$$\Delta G(r,c) = \frac{4}{3}\pi r^2 c (\Delta g^{ch} + \Delta g^{str} + g^{str}_p) + 2\pi r^2 \gamma. \tag{1}$$

The quantities Δg^{ch} and Δg^{str} denote the chemical and strainenergy changes per unit volume, respectively. The value γ denotes the specific interfacial energy of the particle. Together these values are used to define the total free energy change of a transforming martensite particle, where the volume of the particle is expressed in terms of the radius and oblate axis length, r and c. The term g_p^{str} is used to denote an additional strainenergy component accounting for the short range misfit stresses at the austenite-martensite boundary. The values of Δg^{ch} and Δg^{str} are themselves functions of the chemistry and morphology of the martensite being considered. As such, this potential must be specifically defined.

In the current work, the interfacial energy and the boundary misfit strain energy are neglected for simplicity. The strain energy component Δg^{str} must be defined as a function of current

stress state for there to be any coupling between the KMC algorithm and the FEA solution for the stress. This is done using Eshelby's inclusion formulation (Christian, 1975; Pereloma and Edmonds, 2012). For an ellipsoidal region of linear-elastic material undergoing a known internal shape change, the Eshelby formulation provides a closed-form solution for the change in strain energy that occurs. The strain energy change per unit volume is thus given by

$$\Delta g^{str} = -\frac{1}{2}\sigma^I_{ij}\epsilon^I_{ij} - \sigma^A_{ij}\epsilon^I_{ij}. \tag{2}$$

The variable ϵ_{ij}^t represents the transformation strain tensor. The stress within the transforming inclusion σ_{ij}^I is obtained from the Eshelby formulation as $\sigma_{ij}^I = \mathbb{C}_{ijkl}(\epsilon_{kl}^c - \epsilon_{kl}^l)$, where the constrained strain of transformation ϵ^c is determined as the product of Eshelby's tensor **S** and the transformation strain: $\epsilon_{ij}^c = S_{ijkl}\epsilon_{kl}^l$. The first term in equation 2 represents the change in strain energy from the transformation strain. The second term of equation 2 is the work performed by the applied stress σ_{ij}^A at that material point. It is through this term that the Magee effect is incorporated into the model—for a given transformation strain ϵ_{ij}^l the current stress state at that material point may add or remove energy from the system.

Incorporating the result from the Eshelby formulation, dropping surface and boundary misfit strain energy terms, and expressing the potential as a function of volume, equation 1 can be rewritten as

$$\Delta G(V) = V \Delta g^{ch} - V(\frac{1}{2}\sigma_{ij}^I \epsilon_{ij}^t + \overline{\sigma_{ij}^A} \epsilon_{ij}^I). \tag{3}$$

Due to the use of the Eshelby solution, it is important to note that the current model assumes that nuclei geometries are ellipsoidal (though we assume spheroidal inclusions in this work), and that the initial shape change of the new martensite particle happens in a linear-elastic environment (or that the linearelastic assumption provides a good approximation of the strain energy change for a transforming martensitic particle). Recent work by Vasoya et al. (2019) on the energy dissipation rate of Eshelby inclusions may have implications for the linear-elastic assumptions used here. Finally, the value of Δg^{ch} is taken directly from Kaufman and Cohen's work (Kaufman and Cohen, 1958), and the value is chosen for pure iron at a temperature of 300 K. The value of Δg^{ch} for pure iron is chosen here both for simplicity and on the basis that the values of Δg^{ch} reported by Kaufman and Cohen (1958) for simple carbon steels do not differ greatly from those of pure iron for the concentrations of carbon found in most TRIP steels.

As a kinetic event, the nucleation of martensite within metastable austenite requires a certain activation energy to occur. Described in terms of the energy state of a nucleation system, the transformation from the current meta-stable state to the transformed state requires that the system first pass through an intermediate state referred to as the activated, or transition, state. The activation energy is the required energy to get to this intermediate state. Figure 1 depicts a schematic of this process, denoting the meta-stable state as state A, the activated state as

state B, and the final transformed state as state C. The activation energy, or the barrier to transformation, is expressed as the quantity ΔE_{AB} .

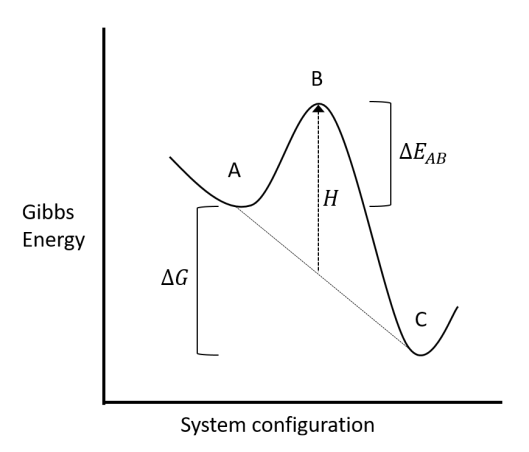


Figure 1: A schematic representing a thermally activated event. As the system evolves from state A to state C, the system must first pass through the activated state B. The barrier height ΔE_{AB} is a function of ΔG (the overall change in free energy between states A and C) and the intrinsic energy barrier H.

In this work the barrier height ΔE_{AB} for a given martensite nucleation event is chosen to be a simple function of the overall change in Gibbs free energy ΔG that accompanies that particular event. This function defines the barrier height as the value H(V) added to a half of the change in Gibbs energy

$$\Delta E_{AB} = \frac{\Delta G(V)}{2} + H(V) \tag{4}$$

The function H(V) = hV is considered to be an intrinsic energy barrier that must be overcome for transformation and has significant effect on the behavior of the model. The per-volume quantity h is chosen as a tuning parameter of the model to fit experimental data. As this is a new model and we seek to focus first on understanding the role of the terms discussed previously, we elect to use fixed values for both h and V, which are defined in a subsequent section. This assumes that the phase transformation for each region must overcome the same barrier, h, although it does account for the bias of the local stress for each of these events in the quantity ΔE_{AB} . This is consistent with other KMC models that use fixed barrier heights to consider martensitic transformations (Chen and Schuh, 2015), lattice-based models where an event barrier is the same for each event (Voter, 2007), and other shear-based deformations (Homer and Schuh, 2009). But it should be noted that H(V) can be defined to incorporate any number of relevant state variables as a model seeks to incorporate greater complexity (Caspersen and Carter, 2005; Hsu (Xu Zuyao), 2006).

2.1.2. Crystallographic model of the martensite transformation

The martensite transformation is defined in the PTMC as an invariant-plane deformation, consisting of a shear parallel to,

and a dilatation normal to, the habit plane (Wechsler et al., 1953; Bowles and Mackenzie, 1954). This can be expressed mathematically to define the transformation deformation gradient

$$\mathbf{F_t} = \beta_t \hat{\mathbf{b}} \otimes \hat{\mathbf{m}} + \mathbf{I},\tag{5}$$

which is a function of the shape strain unit vector $\hat{\mathbf{b}}$, the shape strain magnitude β_T , the habit plane unit normal $\hat{\mathbf{m}}$, and the identity matrix I (Turteltaub and Suiker, 2006; Tjahjanto et al., 2008).

The morphology of martensite that is assumed to form here is lath martensite, typically having a habit plane close to $(5\,5\,7)$ (Sandvik and Wayman, 1983a; Morito et al., 2006; Kelly, 2006). Several past works (Sandvik and Wayman, 1983a,b,c; Kelly, 1992, 2006; Morito et al., 2003, 2006) have studied lath martensite, describing the internal shape change that this morphology of martensite undergoes. Morito et al. (Morito et al., 2003) express the habit plane normals $\hat{\mathbf{m}}$ and the shape strain vectors $\hat{\mathbf{b}}$ for a lath martensite as a function of the lattice parameters for austenite/martensite in pure iron, as well as two slip systems that must activate within the transforming particle to accommodate the deformation. These results are tabulated, and the transformation system Morito reports is given by

$$\hat{\mathbf{m}} = (0.49714 \ 0.71113 \ 0.49714)_{\gamma}$$

$$\hat{\mathbf{b}} = [-0.20113 \ 0.70712 \ -0.67789]_{\gamma}$$

$$\beta_t = 0.24223$$
(6)

By cubic symmetry, the values for $\hat{\mathbf{m}}$, $\hat{\mathbf{b}}$, and β_t in equation 6 result in N=24 variants of martensite having an orientation relationship with its parent austenite that is close to the Kurdjumov-Sachs orientation relationship. The deformation gradients for each of these 24 variants are defined by these vectors via equation 5, which in turn defines 24 different transformation strains ϵ_{ij}^t . As these strains represent different changes in shape, the varying values of ΔG and ΔE_{AB} for each variant give rise to the Magee effect. For more detailed information on the general crystallography of martensite in steel, as well as the crystallography of lath martensite, see Appendix A.1.

2.1.3. The kinetic Monte Carlo algorithm

The kinetic Monte Carlo algorithm serves as the core of the current model, controlling when potential martensite nuclei activate and which martensite variant forms. The KMC algorithm lists all possible nucleation events for the model in its current state and then selects a single nucleation event for activation using the values ΔG and ΔE_{AB} calculated by equations 3 and 4. The KMC algorithm also determines how far the model steps in time with each iteration. The details of the algorithm are presented here. A thorough presentation of the algorithm is given by Voter (2007).

The rate for a single kinetic event is given by

$$k_{AC} = \vartheta \exp\left(\frac{-\Delta E_{AB}}{k_B T}\right). \tag{7}$$

The value k_{AC} is the rate at which the model can be expected to transition from state A to state C (see figure 1). The attempt frequency ϑ is usually taken as the Debye frequency for atomic processes in a lattice. The value of ΔE_{AB} is expected to be a positive value (calculating a rate for a barrierless process is meaningless); the value of the exponential is a probability, and is so capped at 1. As such, the maximum rate at which a process can occur is the attempt frequency. The values k_B and T are the Boltzmann constant and temperature in Kelvin.

For n possible events, the KMC algorithm calculates their rates and subsequently chooses one event to occur. The rates for all n events, listed by k_n , can be used to create an array of normalized partial sums

$$s(j) = \frac{1}{k_{tot}} \sum_{q=1}^{j} k_q \text{ for } j = 1...n,$$
 (8)

where k_{tot} is the total sum of all rates $\sum_{q=1}^{n} k_q$. The result is a list of values ranging from 0 to 1 in increasing order. The values in this array are used to select which event occurs for the next step of the model's evolution. The magnitude difference between elements s(j-1) and s(j) is proportional to the rate calculated for event j. An event is selected by generating a random number ξ_1 from a uniform distribution and determining where in the array s(j) that number falls. If ξ_1 falls within the range set by elements s(j-1) and s(j) then event j is selected to occur. Using this method, events with the larger kinetic rates have a higher probability of being selected to occur.

The model also advances in time according to the kinetic rates calculated for all possible events. The sum of all rates k_{tot} and another random number ξ_2 (from a uniform distribution) are used to generate an exponentially distributed random number Δt , the time increment stepped forward by the model. This is calculated as $\Delta t = -\ln \xi_2/k_{tot}$. The model is then stepped forward in time, the chosen event occurs, the system's energy state is changed accordingly, and the process is repeated with the next set of possible events.

The KMC method typically allows transformations to reverse themselves, as a model may select to return to its previous state. This typically occurs when an energetically unfavorable event was selected at low probability, resulting in the reverse transformation having a high rate of occurrence in the next step. A modified KMC approach is taken here, however, where events are prohibited from being chosen if there are no events present that have kinetic rates over some chosen threshold value. This is a useful approach when the total sum of all possible transformation rates is close to zero, resulting in an unrealistically large time step and dramatic model behaviors. This is done either by setting a minimum total rate k_{tot} , or by setting a maximum time step Δt ; if either condition is not met, no transformations are selected and the model steps forward in time by the maximum allowed step. This allows the model to evolve according to external constraints, changing the energy state of the model and moving toward a set of more acceptable transformation events.

2.2. Model implementation

In the present manuscript we examine two different KMC model implementations to observe the effects of load path and the kinematic coupling between austenite regions on the nucleation behavior of martensite. The core of the nucleation model consists of the KMC algorithm's calculation of kinetic rates in potential martensite nucleation events given the equations described in sections 2.1.3 and 2.1.1. Finite element analysis with appropriate boundary conditions allows the simulation of different load paths that can be used to examine the influence of applied stresses on nucleation kinetics. The two implementations of the model differ in how kinematic coupling affects the kinetics of martensite nucleation, contrasting the roles played by both kinematic coupling and load path. One model is referred to as the "virtual" model, and the other as the "fully-coupled" or "KMC-FEA" model.

Both implementations of the model track the transformation of 20 nuclei, representing preexisting sites for the heterogeneous nucleation of martensite. Each nucleus is assigned an austenite orientation taken from a random distribution, and the appropriate rotations are applied to the transformation strains defined by equations 5 and 6 for the different variants of martensite that can form there. The same set of 20 orientations is used across all implementations and runs of the KMC algorithm to remove the effect of changing texture on the model and isolate the effects of load path and kinematic coupling. As each implementation of the model progresses, the KMC algorithm chooses which nucleus transforms, and to what variant. Both implementations of the model require the solution of an FEA model for the defining of stresses as the model progresses. Since the two model implementations have common elements, we begin by first describing the FEA constitutive behaviors and boundary conditions that were used. This is followed by a description of each model implementation.

2.2.1. FEA constitutive behavior and boundary conditions

The effects of load path on nucleation are achieved through the boundary conditions applied to various FEA meshes. Each implementation of the model utilizes an FEA mesh that simulates a cubic region of matrix material initially containing spheres of retained austenite. For each meshed cubic volume, three sets of displacement boundary conditions (DBC) and fixed boundary conditions (FBC) are placed on the model. Uniaxial loading is achieved by a DBC on the positive x face of the simulation cube, with FBCs placed on the negative x, y, and z faces. Biaxial loading is achieved by DBCs on the positive xand y faces, again with FBCs placed on the negative x, y, and zfaces. Finally, plane strain loading is achieved by a DBC on the positive x face, with FBCs placed on both y faces as well as the negative x and z faces. Each displacement boundary condition progresses at the set strain rate of $\dot{\epsilon} = 0.001 \ s^{-1}$ and continues until all 20 austenite regions have transformed. The equivalent strain is used to represent the bulk strain state of the simulation region during deformation, and serves as a basis of comparison across the different load paths. The equivalent strain is defined

as

$$\bar{\epsilon} = \sqrt{\frac{2}{3}\epsilon^{\text{dev}} : \epsilon^{\text{dev}}},$$
 (9)

where ϵ^{dev} is the deviatoric strain defined by $\epsilon^{\text{dev}} = \epsilon - \frac{1}{3} \text{tr}(\epsilon) \mathbf{I}$. The material constitutive behaviors used in the FEA analysis follow the assumptions outlined in section 2.1. Plasticity in the austenite is neglected and the plasticity in the transformed martensite is included only as a portion of the deformation gradient F_t as defined by Morito et al. (2003). The matrix material is allowed to plastically deform via Mises plasticity. For speed and simplicity perfect plasticity is assumed, with a yield strength of 1180 MPa. The FEA constitutive model for both austenite and mechanically induced martensite is isotropic linear elasticity, with Green strain and the 2nd Piola Kirchoff stress as energetic conjugates. For transforming martensite, the stress is calculated as a function of the end-of-increment deformation gradient $\mathbf{F}_{\tau+\Delta\tau}$, where τ is the simulation time at the beginning of the increment. A multiplicative decomposition of the endof-increment deformation is assumed to consist of elastic and

$$\mathbf{F}_{\tau+\Delta\tau} = \mathbf{F}_{\mathbf{e}}\mathbf{F}_{\mathbf{t}},\tag{10}$$

where \mathbf{F}_t is the transformation defined for a given variant of martensite. The Green strain at the end of the increment is given by

transformative parts. This decomposition is given as

$$\mathbf{E} = \frac{1}{2} (\mathbf{F}_{\mathbf{e}}^{\mathbf{T}} \mathbf{F}_{\mathbf{e}} - \mathbf{I}). \tag{11}$$

The 2nd Piola Kirchoff stress is given as

$$\sigma^{\mathbf{PK}} = \mathbb{C}\mathbf{E} \tag{12}$$

The stiffness tensor $\mathbb C$ is isotropic, defined by a Young's modulus of E=200 GPa and a Poisson's ratio of ν =0.3 (Cantara et al., 2019). The Cauchy stress is subsequently defined as

$$\sigma = \frac{1}{\det(\mathbf{F}_e)} (\mathbf{F}_e \sigma^{\mathbf{PK}} \mathbf{F}_e^{\mathbf{T}})$$
 (13)

The model is solved implicitly, requiring a Jacobian matrix to bring the solution into convergence. The Jacobian used here follows the perturbed Jacobian method used by Kalidindi et al. (1992). The KMC-FEA model runs in ABAQUS/standard version 6.11 with the implicit FEA solver. The type of element used in all cases is C3D10 (quadratic tetrahedral elements). The mesh, material constitutive behavior, KMC algorithm, and post processing of results are all managed via the use of user subroutines UMAT and UEXTERNALDB, as well as ABAQUS scripting tools.

As noted earlier, we choose to implement two different versions of the model to study the effects of load path and kinematic coupling in different ways. These two implementations utilize different FEA models and execute the calculations of the KMC algorithm differently. The virtual model isolates the effect of load path by pre-solving an FEA model containing a single austenite sphere to tabulate the stresses caused by each load path that are used in the KMC algorithm. These pre-tabulated

stresses for different load paths are then used to track martensite transformation at the 20 nucleation sites in isolation (i.e. with no kinematic coupling between nuclei), using the same calculated stresses for each nucleus. The KMC-FEA model solves an FEA model with each of the 20 nucleation sites contained in a single volume. This allows the effects of each transformation to propagate through the model's evolution via the KMC algorithm and captures the effects of both load path and kinematic coupling.

All model inputs required by the KMC algorithm are summarized and listed in table 1. More specific details of each implementation are presented in the following sections.

2.2.2. The virtual transformation model

The virtual model simulates the transformation of 20 martensite nuclei by executing the KMC algorithm within the MAT-LAB environment. The KMC algorithm controls the evolution of the model following the steps outlined in section 2.1.3, and given in algorithm 1. Since this model is carried out in MAT-LAB instead of in an FEA environment, the stresses for each load path are pre-tabulated. These stresses are referenced by the KMC algorithm as it steps forward in time to calculate the relevant kinetic rates for each possible nucleation event. As a nucleus is selected to transform to one of the 24 variants of martensite, the conditions of its transformation are recorded and it is removed from the list. This also means that there is no physical effect on the model once each nucleus transforms. These "virtual" transformations are counted until all 20 nuclei have been selected to transform. The model output of interest is the equivalent strain at which each of the 20 nuclei transform.

To obtain the pre-tabulated stresses, an FEA model consisting of a single linear-elastic austenite sphere embedded in a plastic matrix is subjected to uniaxial, biaxial, and plane strain loading conditions. The stresses inside the nucleus are tabulated as a function of equivalent strain for each loading path. The material constitutive behaviors and boundary conditions follow the descriptions in section 2.2.1.

The virtual model serves several functions in the study of martensite nucleation. First, the model runs quickly and can therefore provide a statistical understanding of how load path affects martensite nucleation through observation of results for many runs. In comparison, the KMC-FEA model cannot provide the same statistical insight because it requires an FEA solution with every time step.

Second, the stochastic nature of the KMC algorithm provides insight into the probabilities of a system evolving in different ways; each run yields a unique result, and lots of runs provide insight into the variation of the output where a deterministic model would yield the same output each time. This can be used to study how sensitive certain outcomes are to initial conditions.

Third, the virtual model isolates the effect of load path. Since the transformation of each nucleus is not explicitly modeled, the only effect of stress on transformation is from stresses caused by the boundary conditions on the pre-solved FEA model. The virtual model provides an important point of comparison with the KMC-FEA model, as it removes any effect of kinematic coupling.

Table 1: KMC Parameters

Property	Symbol	Value	Ref.
Number of Variants	N	24	
Habit Normal	ŵ	$(0.49714 \ 0.71113 \ 0.49714)_{\gamma}$	(Morito et al., 2003)
Shape Strain Vector	ĥ	$[-0.20113 \ 0.70712 \ -0.67789]_{\gamma}$	(Morito et al., 2003)
Shape Strain Magnitude	β_t	0.24223	(Morito et al., 2003)
Elastic Modulus	\boldsymbol{E}	200 GPa	
Poisson's Ratio	v	0.3	
Strain Rate	$\dot{\epsilon}$	0.001	
Nucleate Volume	V	$1.2 \times 10^{-4} \ \mu \text{m}^3$	
Maximum KMC Time Step	Δt_{max}	1 sec	
MIMT Chemical Free Energy Change	Δg^{ch}	$-5.629 \times 10^{-4} \frac{N}{\mu m^2}$	(Kaufman and Cohen, 1958)
Intrinsic Energy Barrier	h	$1.0 \times 10^{-3} \frac{N}{\mu m^2}$	
Nucleation Attempt Frequency	ϑ	$1.59666 \times 10^{13} \text{ Hz}$	7
Temperature	T	300 K	

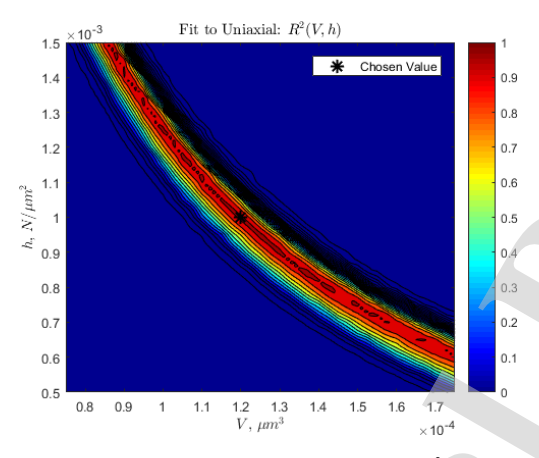


Figure 2: A contoured representation of the dependency of \mathbb{R}^2 (the fit of the average output of the virtual model to data provided by Ennis et al. (2017)) on the values h and V for the uniaxial load path.

Finally, the virtual model is used to choose the values of nucleus volume V and the barrier height term h required by the KMC algorithm. This is done by fitting the averaged output of the virtual model to experimental data provided by Ennis et al. (2017). For the uniaxial load path, the virtual model is run 20 times and the results averaged. The averaged results are compared to the experimental data for that load path and the R^2 value is calculated as the measure of fit quality. To obtain the V and h values used in this work, the value for V was initially chosen and the value for h was chosen to produce an H in the same order of magnitude of the value for ΔG for such a nucleus transforming at zero applied stress (where all variants will have the same value of ΔG). This resulted in the following values, $V = 1.2 \times 10^{-4} \ \mu \text{m}^3$ and $h = 1.0 \times 10^{-3} \ \text{N}/\mu \text{m}^2$.

A subsequent search around the neighborhood of this initial choice shows a particular relationship between values of h and V that provide good fits to experimental data. Figure 2 depicts this neighborhood of h and V, showing the R^2 values that result

from fitting the output of the virtual model to the data provided by Ennis et al. (2017), using each combination of h and V. Each data point in figure 2 represents the comparison of Ennis' data to the average of 20 runs of the virtual model under uniaxial loading. This figure shows that the choice of intrinsic barrier height h is still sensitive to the choice of V, showing that the nucleation kinetics are not dominated by the choice of V alone. For this reason, the first manually-determined estimate of the parameters h and V are kept as the final values. The comparison of these fit curves to the experimental data are given and examined in the results section.

2.2.3. KMC-FEA coupled model

In contrast to the virtual model where the stresses are pretabulated, the KMC-FEA model involves a full solution of the stress field in every step as boundary conditions progress through each load path. Furthermore, whereas the virtual model has a list of 20 austenite regions, the KMC-FEA model geometry contains all 20 regions of austenite phase embedded in the matrix material. Each of the 20 austenite regions is represented as an idealistic sphere with a set volume of 0.04 μm^3 . Each sphere contains one of the 20 nucleation sites which is assumed to produce a nucleus having a volume of V as determined using the virtual model. When a given nucleation site is selected by the KMC algorithm to transform, the entire spherical austenite grain that contains it undergoes the corresponding change in shape. The crystallographic orientations of these spherical austenite grains correspond with the orientations assigned to their respective nuclei. The FEA geometry for the model is depicted in figure 3. These material constitutive models follow the behaviors outlined in section 2.2.1 for the respective phases. A detailed description of the KMC-FEA model is given in algorithm 2.

This KMC-FEA model implementation is used to study the effect of kinematic coupling, or interaction between martensite transformations, by varying the volume of the cube that contains the austenite grains. Three different cube volumes are used $(10, 20, \text{ and } 40 \, \mu \text{m}^3)$, with extra padding to distance the austenite regions from the boundary conditions. The spheres repre-

Algorithm 1 Virtual Transformation Model

```
1: Run FEA model containing single austenite sphere for the
     given strain path and tabulate \sigma^A(t) and \bar{\epsilon}(t).
 2: Set the orientations of 20 nuclei
 3: t = 0, N_{nuc} = 20
 4: while N_{nuc} > 0 do
         Interpolate \bar{\epsilon} from \bar{\epsilon}(t)
         Interpolate \overline{\sigma^A} from \overline{\sigma^A}(t)
 6:
 7:
         for each nucleus do
              for each martensite variant do
 8:
                   Calculate k (eqns. 3, 4, and 7)
 9:
                   Add k to list k_n
10:
              end for
11:
12:
         end for
         Calculate k_{tot} = \Sigma k_n
13:
14:
         Generate random numbers \xi_1 and \xi_2
         Calculate \Delta t = -\ln \xi_2/k_{tot}
15:
16:
         if \Delta t \geq \Delta t_{max} then
              t = t + \Delta t_{max}
17.
18:
              Calculate array of partial sums s(j) (eqn. 8)
19.
20:
              Choose event j such that \xi_1 \in [s(j-1), s(j)]
21:
              Remove nucleus from list of possible nuclei
22:
              N_{nuc} = N_{nuc} - 1
              t = t + \Delta t
23:
         end if
24:
25: end while
```

senting austenite are randomly placed throughout the cube. As the same 20 austenite grains are used in each case, the relative differences in spacing affect the influence previous transformations have on future martensite nucleation, as communicated through the evolving stress fields.

3. Results

The results of both the virtual and fully coupled models are outlined here in their respective sections. The virtual model shows a difference in how the bulk stress states caused by each load path (uniaxial, biaxial, and plane strain) affect the nucleation of martensite differently. The virtual model does not include any notion of kinematic coupling, and so isolates the effect of load path on martensite nucleation. The fully coupled KMC-FEA model includes both the effects of load path and kinematic coupling of adjacent austenite regions. The effect of kinematic coupling is shown by applying the KMC-FEA model to simulated materials that contain austenite regions dispersed at different spacings, resulting in different transformation rates. Here, the term "transformation rate" denotes the rate at which austenite regions transform with respect to equivalent strain. This is to distinguish this term from the "kinetic rate", which is a temporal rate as calculated by the KMC algorithm.

3.1. Virtual transformation model

The virtual transformation model was used to simulate the transformation of 20 virtual nuclei at sites having pre-selected

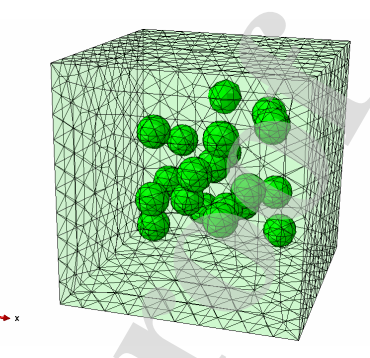


Figure 3: A simulation cell of $10~\mu m^3$ containing twenty $0.04~\mu m^3$ austenite regions represented by randomly placed idealistic spheres. This volume is contained within a region of surrounding material, providing a buffer from applied boundary conditions. Grain orientations are assigned to each austenite region from a set of orientations previously generated from a random distribution.

orientations. Here, the virtual model was run 20 times for each load path. The results of the virtual model are plotted in figure 4 along with the experimental data for austenite transformation provided by both Ennis et al. (2017) and Cramer et al. (2018). The curves representing the fraction of remaining austenite are the averages of the 20 runs for each load path. The relative comparison of the shapes of these curves is given in the final panel of figure 4. The uniaxial and biaxial load cases are separated from each other, with uniaxial loading causing transformation of austenite faster with respect to equivalent strain. The plane strain load case aligns with the uniaxial load case for a short period (approx. 2% strain) before separating to run nearly parallel to the biaxial load case. The uniaxial case has the most dramatic change from a high transformation rate to a low oneevidenced by the severity of the "elbow" in the transformation curve. The plane strain case has the least severe elbow. These elbows signify that one or more austenite regions do not transform as readily as the others, slowing the rate of austenite trans-

Figure 4 also displays the 1 standard deviation range for the 20 runs of the virtual model for each load path. Since each run uses the same 20 austenite orientations, the statistical variance of the results for a given load path is purely a function of the stochasticity of the KMC algorithm, demonstrating the considerable variation of possible results from the same initial microstructure.

As noted, figure 4 also compares the results of the virtual model to experimental data. Since the virtual model tracks the transformation of a discrete number of nuclei, the transformation of austenite is compared with experimental data via the fraction of austenite remaining. As the data provided by Ennis et al. (2017) was used to validate the virtual model, the average of the uniaxial runs of the virtual model fits well, having an R^2 of 0.984. The plane strain and biaxial cases fit the experimental data provided by Cramer et al. well, with R^2 values of 0.988 and 0.976, respectively. The uniaxial case deviates very quickly from a good fit to Cramer's data, however, with an R^2 value of 0.652. It is likely that some of the RA levels seen

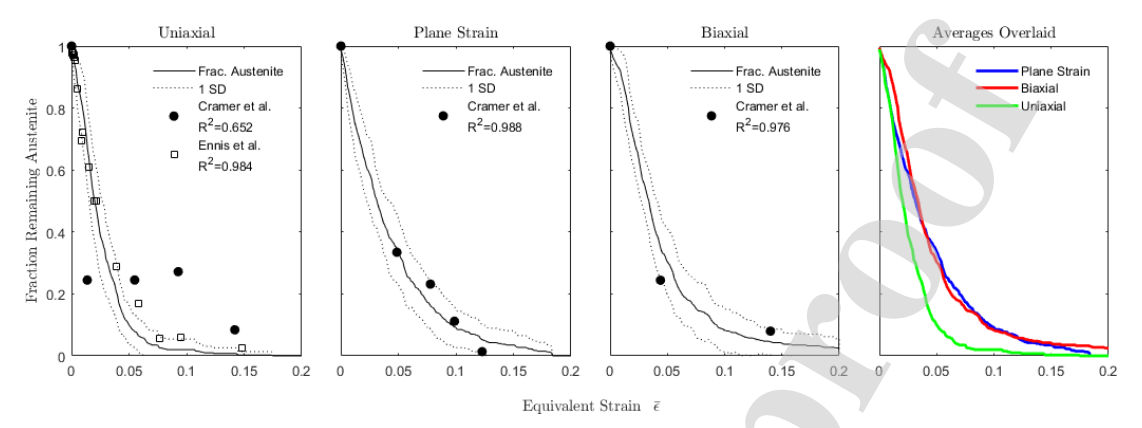


Figure 4: Results of the virtual model, each curve representing the average of 20 runs of the virtual model and tracking the transformation of 20 austenite nuclei.

in Figure 4 are not accurate for uniaxial tension; the authors Cramer et al. (2018) have seen a smoother transformation rate for uniaxial tension in subsequent in-situ experiments for Q&P 1180 (Miles, 2019).

3.2. KMC-FEA coupled model

The results of the fully coupled KMC-FEA model are shown in figure 5, which depicts the number of remaining martensite nucleation sites as a function of equivalent strain. Results are grouped by the average nearest-neighbor distance between austenite regions, corresponding with simulation cells having volumes equal to 10, 20, and 40 um³. Resulting average nearest neighbor distances between the austenite regions are $\overline{NN} = 0.555$, 0.751, and 0.908 μm respectively, the space between austenite regions increasing as they are distributed through larger volumes. Each curve represents the average of two KMC-FEA model runs. Additionally, each data set is fit by a sigmoid curve having the form of $-a \tanh(bx) + c$; each respective R^2 value is listed. The relationship between the uniaxial and biaxial load paths seems to be fairly consistent with changing value of \overline{NN} ; the uniaxial case shows faster transformation with respect to equivalent strain when compared with the biaxial load path in all cases. The relationship between uniaxial and plane strain load paths is more varied, however. An example of this can be seen in observing points at which the plane strain curve crosses the uniaxial curve for each case in figure 5—as \overline{NN} increases, the first crossing point happens at earlier and earlier equivalent strains.

The transformation rates, or rate of change of the retained austenite fraction as a function of equivalent strain, are calculated from the slopes of the sigmoid curves used to fit the data in figure 5. These slopes, or transformation rates, are plotted as a function of the equivalent strain in figure 6. The effect of \overline{NN} on transformation rate is shown for each load path. For comparison, the transformation rates observed in the virtual model are also included in figure 6.

For the plane strain load path, the transformation rates shown in figure 6 exhibit a trend in which the fully coupled model behaves more and more like the virtual model under plane strain loading with increasing \overline{NN} . In other words, with increasing space between austenite regions the initial nucleation rate under plane strain loading decreases in magnitude to behave more like the virtual model, which has no kinematic coupling.

Under biaxial loading, the magnitude of the transformation rates seem to be minimally affected by an increase in \overline{NN} , with transformation rate curves close to that of the virtual model. The results for biaxial loading do show the same trend, however, of the initial rates of nucleation converging toward the behavior of the virtual model with increasing \overline{NN} .

The uniaxial case shows greater sensitivity to a change in \overline{NN} than the biaxial case, though no ordering of the results with respect to \overline{NN} is observed. This lack of convergence towards the virtual model with increasing \overline{NN} indicates greater randomness to the transformation rates under uniaxial loading.

4. Discussion

The results of both the virtual model and the KMC-FEA coupled model show the effect of load path and kinematic coupling on the transformation rates of martensite. The virtual model, used to validate the KMC parameters by comparison to experimental data, shows how the effect of load path on nucleation originates from the Magee effect–different stress states imposed by different boundary conditions encourage/suppress each of the 24 martensite variants differently. The fully coupled model shows how kinematic coupling, or changes in \overline{NN} , affect transformation rate differently for each load path. In short, the Magee effect sets each load path apart from each other, which results in different sensitivities to kinematic coupling. The comparison of the virtual model results to experimental data is discussed first. The role of the Magee effect is then discussed, followed by the role of kinematic coupling in each load path.

4.1. Comparison to experimental data

The data provided by Ennis et al. (2017) and Cramer et al. (2018) provide important context for present results. The model was primarily validated by Ennis' experimental data, and only

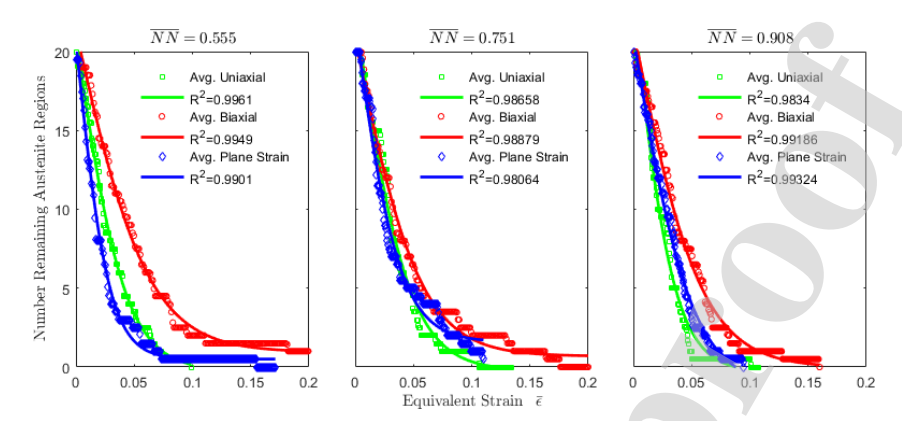


Figure 5: Results of the FEA-KMC coupled model for simulation cells of different volumes, with the same volume of austenite distributed throughout.

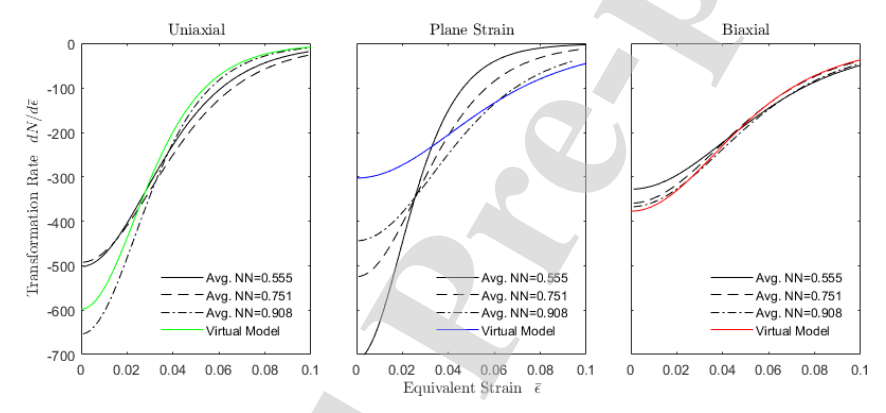


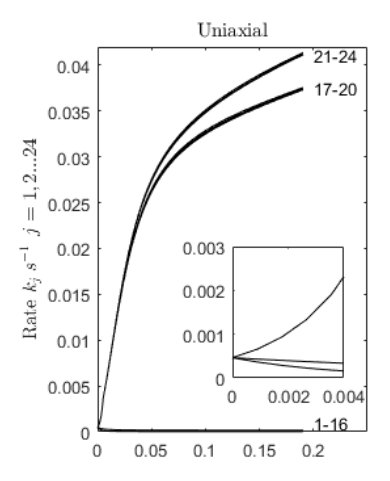
Figure 6: Transformation rates for the fully coupled FEA-KMC and virtual models. Results are grouped by load path, demonstrating the effect of austenite spacing on the transformation rate for each case.

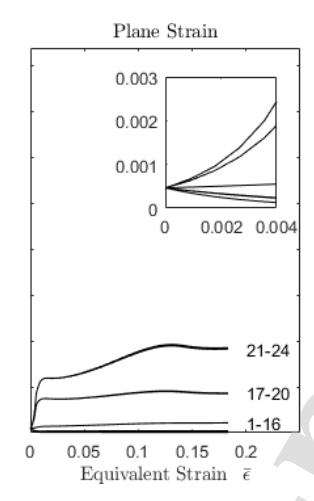
compared to the data presented by Cramer. Aspects of both materials were used as a basis for model constitutive behaviors, with the bulk of assumptions being derived from Ennis' conclusions; the primary assumption being the isothermal stress-assisted nucleation of martensite. Ennis presents data for the case of uniaxial deformation of TADP steel, concluding that this material undergoes the isothermal stress-assisted nucleation of martensite. For this reason Ennis' data is presented primarily as validation of the current model. The uniaxial data provided by Ennis represents measurement of austenite volume fractions as measured by X-ray diffraction, and so provides a statistically significant volume of data well suited for validation of the input parameters of the models presented here.

The comparison of present results to the data provided by Cramer et al. has implications regarding possible relationships between stress-assisted and strain-induced martensite nucleation. Q&P steels are generally assumed to undergo the strain-induced martensite transformation, as their M_s^{σ} is usually reported to be well below room temperature (De Moor et al., 2008; Wang and Speer, 2013). The excellent fit of the virtual model to Cramer's data in the plane strain and biaxial

cases may suggest a greater role of stress-assisted nucleation kinetics in Q&P. Both modes of nucleation may happen in any material, and the primary task in defining M_s^{σ} is one of determining which nucleation mode is most dominant for a given temperature range. Other microstructural features may affect how and when retained austenite deforms, and so stress-assisted nucleation of martensite may be happening within the material studied by Cramer. Additional confirmation of the mode of nucleation within the alloy studied by Cramer may be achieved through the observation of ε -martensite shear bands directly. The comparison of present results to the uniaxial data provided by Cramer are suspect, primarily due to concerns about how that data was gathered (Miles, 2019).

In any case, while the model is derived from characteristics of these materials, it is a model and is internally self consistent. Regardless of any implications that arise from comparison to these data, the results represent how both the Magee effect and kinematic coupling affect nucleation kinetics within the virtual and KMC-FEA models.





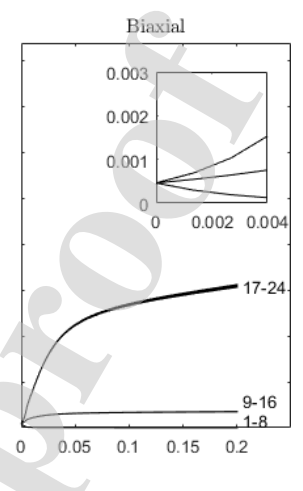


Figure 7: The rates of transformation for each of the 24 variants of martensite for a single nucleation site under each load path. The grain orientation of the austenite nucleation site is unrotated from the reference frame. Numbers depict how the 24 variants are grouped within each cluster of curves.

4.2. Role of the Magee effect

The Magee effect underlies the differences in transformation rates between all 24 variants via the interaction of the applied stress field with the stress field that results from the martensite transformation. Due to the strain energy dominated nature of martensite nucleation kinetics, the transformation rates are sensitive to the stress state caused by imposed boundary conditions as well as more local stresses caused by adjacent transformations. As such, the Magee effect provides a useful framework for the description of present results. The calculations within the KMC algorithm further add useful means of quantifying the Magee effect, through the calculation of kinetic rates.

Figure 7 depicts the kinetic rates of transformation for all 24 variants of martensite for a single potential nucleus. Each load path, with their respective differences in imposed stress state, result in different "spectra" of kinetic rates. These spectra lead to different groupings of the variants, as well as their corresponding magnitudes of kinetic rates, as a function of equivalent strain. The plane strain spectrum shows 6 groups of 4 variants each, distributed over a smaller range of kinetic rates when compared to biaxial and uniaxial load cases. Three of these groups experience a positive energetic bias (are assisted) while the other three experience a negative energetic bias (are suppressed). The biaxial case shows 3 groups of 8 variants each, of which only one group is suppressed. The uniaxial case also shows 3 groups of 8, but two of the three groups are suppressed.

It is important to note that these spectra are a function of the orientation of the austenite crystal where the potential nucleus is located, and spectra for only one orientation are shown here. As this orientation is changed, the curves in each spectrum "rotate" between states of being suppressed and assisted in various magnitudes. The grouping of variants into concentrated bands within the spectrum is also a function of the orientation of the nucleus. This suggests that a mapping between the space of nucleus orientations and the space of resulting spectra can be

created—such a mapping could be used to study or even control how retained austenite texture affects the kinetics of the stress-assisted nucleation of martensite.

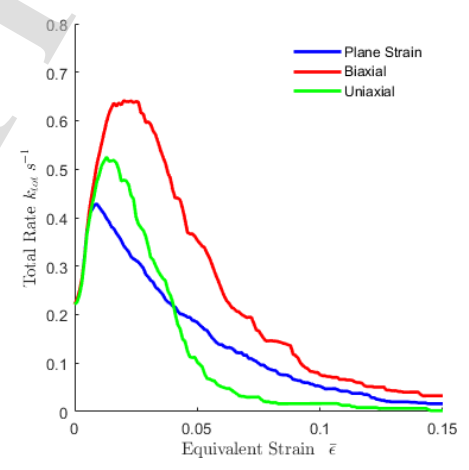


Figure 8: Representation of the total kinetic rate k_{tot} as a function of equivalent strain for each load path, as calculated in the virtual model. The magnitude of the total rate at a given equivalent strain corresponds with the rate of any austenite transformation event occurring.

The overall effect that these differing variant spectra have on the nucleation behavior of martensite can be demonstrated by considering the total kinetic rate k_{tot} , or sum of all the individual rates in the spectra as calculated by the KMC algorithm. Figure 8 plots the total kinetic rate as a function of equivalent strain for each load path, as calculated for the virtual model. As such, it includes not only the effects of the different spectra, but the case where a range of orientations can uniquely contribute to the rates. The shape of the curves gives insight into the different stages of martensite nucleation behaviors that are

Algorithm 2 KMC-FEA Model

```
1: Load FEA mesh containing 20 austenite spheres in a cube
    of matrix material
 2: t = 0, N_{nuc} = 20
 3: while N_{nuc} > 0 do
        for each nucleus do
             for each martensite variant do
 5.
                 Calculate k (eqns. 3, 4, and 7)
 6:
 7.
                 Add k to list k_n
 8:
             end for
        end for
 9:
10:
        Calculate k_{tot} = \Sigma k_n
11:
        Generate random numbers \xi_1 and \xi_2
12:
        Calculate \Delta t = -\ln \xi_2/k_{tot}
13:
        if \Delta t \geq \Delta t_{max} then
14:
             t = t + \Delta t_{max}
             Step DBCs forward at \dot{\epsilon} = 0.001
15:
16:
             Solve FEA time step for stresses in cube
17:
             Calculate array of partial sums s(i) (eqn. 8)
18:
19:
             Choose event j such that \xi_1 \in [s(j-1), s(j)]
             Remove nucleus from list of possible nuclei
20:
21:
             N_{nuc} = N_{nuc} - 1
             t = t + \Delta t
22:
             Step DBCs forward at \dot{\epsilon} = 0.001 s^{-1}
23:
24:
             Set \epsilon_t for elements of sphere containing nucleus
25:
             Solve FEA time step for stresses in cube
        end if
26:
27: end while
```

governed by competing factors. The first stage is an increase in total kinetic rate as stress increases during initial linear elastic loading, the beginnings of plasticity, and the initial transformation of austenite regions. During this early loading, each load path shows a similar trajectory at early strains, overlapping until approximately 2% equivalent strain. Each load path eventually comes to a peak where the nucleation of assisted variants outpaces the overall increase in kinetic rate as potential nuclei are taken out of the pool of events contributing to the total. The following stage, representing a decay of the total rate as variants nucleate, demonstrates the effect of the differing spectra for each load path: The plane strain case having the most gradual decay as a result of the greatest number of variants in the spectra that are assisted by the stress state. Because the uniaxial load path assists only a few variants, the total kinetic rate decays much faster as the assisted variants are selected to nucleate. The biaxial case represents a more balanced combination of assisted variants at a high rate, thus having the highest peak and a rate of decay intermediate to that of the uniaxial and plane strain cases. In short, the biaxial load case tends to be the upper bound of the curves plotted in figure 5 due to this balance. The strong preference of a few variants in the uniaxial case is what causes the uniaxial curves in figure 5 to be consistently below the biaxial curves.

4.3. Role of kinematic coupling

The adjacency of austenite regions has a direct impact on the extent to which transformation stress fields interact with each other. This difference can be seen in the different transformation rates for different values of \overline{NN} , as shown in figure 6. This suggests a difference in sensitivity to kinematic coupling across the different load paths. The inclusion of the transformation rates of the virtual model in figure 6 provide an important point of comparison, because the virtual model's behavior represents an absence of any kinematic coupling or $\overline{NN} = \infty$. This comparison elucidates the different roles that kinematic coupling plays in the different load paths.

For the plane strain load case, these plots show different initial nucleation rates with respect to \overline{NN} -suggesting that greater kinematic coupling is responsible for increasing the transformation rate of martensite while under a plane strain load. In other words, with increasing \overline{NN} the magnitude of the initial nucleation rate decreases, and the results of the fully coupled model converge toward the virtual model's behavior. The spread of initial nucleation rates for plane strain is greater than the other load paths, suggesting that martensite nucleation is more sensitive to kinematic coupling under plane strain loading than both uniaxial and biaxial conditions.

The biaxial load path seems to converge to the virtual model's behavior similarly, but over such a narrow range of nucleation rates as to suggest a relative insensitivity to kinematic coupling in comparison with the plane strain load path. The uniaxial load path does not exhibit the same ordering of model behaviors as average nearest neighbor distance changes; the average behavior of the model under plane strain loading across all average nearest neighbor distances is close to the behavior of the virtual model.

In summary, the plane strain load path exhibits sensitivity to the kinematic coupling of adjacent regions (i.e. austenite regions are more likely to transform the closer they are to adjacent transforming austenite regions) while the biaxial and uniaxial load paths remain relatively unaffected by changes in average nearest neighbor distance.

4.4. Application to TRIP-assisted steels

As the strength and ductility exhibited by TRIP-assisted steels are dependent upon the martensitic transformation, we examine how the conclusions of this work might influence the design or expected behaviors of TRIP-assisted steels that exhibit the stress-assisted nucleation of martensite. For such steels under uniaxial or biaxial loading, the general proximity of austenite regions does not appear to accelerate or retard the transformation behavior. As nucleation behaviors appear unaffected by the proximity of retained austenite regions, an increase in volume fraction (and thus a decrease in average distance between austenite regions) may not reduce the range of equivalent strains in which austenite transforms. Because of this, it may be easier to affect the hardening behavior of these steels over large ranges of strain in the case of uniaxial or biaxial loading simply by increasing the initial volume fraction of austenite. On the other hand, Because the plane strain case

exhibits faster nucleation behaviors when austenite regions are close to each other, increasing the volume fraction of austenite may have undesirable effects if the intention is to pace the transformation of austenite over a larger range of plastic strains.

These expected behaviors are, of course, a function not only of the initial volume fraction of austenite but also of other microstructural characteristics that effect the dispersion of austenite: volume of individual austenite regions, austenite grain morphology, etc. Both the virtual model and the KMC-FEA coupled model would provide a good field for the study of texture on the transformation of austenite. Future applications of the model may also study the effects of retained austenite morphology or composite load paths. Additionally, the incorporation of a crystal plasticity method into the model would allow for the Greenwood-Johnson effect to play a role in the model's behavior. More work is required to provide the necessary insight to understand the influence of these other factors.

5. Summary and Conclusions

A KMC based model is employed to study the interrelationship between the kinetics of isothermal stress-assisted martensite nucleation, kinematic coupling of adjacent austenite regions, and deformation through different load paths (plane strain, biaxial, and uniaxial). Two different KMC models are used to explore the effects of both kinematic coupling and load path by comparing their results. In a virtual model, independent transformation events are simply counted as the KMC algorithm progresses using pre-tabulated stresses. The full KMC-FEA coupled model solves for stresses between each iteration of the KMC algorithm, incorporating the effects of both load path and kinematic coupling. The role of kinematic coupling in the fully coupled model is demonstrated by controlling the average nearest neighbor distance \overline{NN} between austenite regions. One can then quantify how the transformation rate differs with applied strain for the different spacing between austenite regions and for the different load paths.

The differences in transformation rate compared across the different load paths can be attributed the Magee effect, where different groups of variants are suppressed/assisted based on the strain path. This suppression/assistance is illustrated by the different "spectra" of nucleation rates for each strain path, which depict how individual variants are affected by the applied stress state. Given these spectra, the isothermal nucleation kinetics of stress-assisted martensite may be a function of the texture of retained austenite.

The results of the fully-coupled KMC-FEA model depict different outcomes for the different load paths as a function of the average nearest neighbor distance \overline{NN} between adjacent austenite regions. The plane strain load path is unique, in that the rate of austenite transformation appears to be more sensitive to the kinematic coupling between adjacent austenite regions as compared with biaxial and uniaxial load paths. The overall trends appear to be consistent with the virtual model, in which the austenite regions are not kinematically coupled.

The design of the model incorporates some aspects of the microstructures of TRIP-assisted steels, namely the amount

of austenite present, the crystallographic parameters of the martensite transformation, and KMC input parameters that were chosen by fitting to experimental data. With respect to TRIP-assisted steels that undergo the stress-assisted martensite transformation, several implications of this model's results include:

- The fraction of austenite transformed during deformation depends on load path, and so hardening behavior under different load paths may vary.
- The kinetics of stress-assisted martensite nucleation differ by load path through the Magee effect, which provides a means of mapping the relationship between nucleation kinetics and applied stress states.
- The rates of transformation of retained austenite in TRIPassisted steels undergoing the stress-assisted martensite transformation can be expressed as a function of the proximity of austenite regions when under plane strain loading, and so hardening behavior under this load path may be possible to influence by controlling kinematic coupling of adjacent austenite regions.
- The biaxial load path is relatively unaffected by the kinematic coupling of adjacent austenite regions, and so may
 be insensitive to many aspects of microstructure, such as
 the relative proximity of austenite regions.

Acknowledgements

This work is supported by the U.S. National Science Foundation under grant no. DMR-1507095. M.K. is supported provided by the U.S. National Science Foundation under grant no. OIA-1757371.

Appendix A. Phenomenological theory of martensite crystallography

Appendix A.1. General crystallography

The various morphologies of martensite can be distinguished by their respective habit planes, and mode of accommodating the deformation that accompanies their change in shape (Christian, 1975; Pereloma and Edmonds, 2012). Thin-plate martensites, comprised of small alternating layers of twinned martensite variants, are often observed to have habit planes close to (3 10 15) in the austenite phase (Turteltaub and Suiker, 2006; Tjahjanto et al., 2008; Pereloma and Edmonds, 2012). This morphology often exhibits the Greninger-Troiano orientation relationship. In contrast is lath martensite, where the habit planes are close to (5 5 7) and the orientation relationship tends towards Kurdjumov-Sachs (Kelly, 1992; Morito et al., 2003, 2006; Pereloma and Edmonds, 2012). During the martensite transformation, significant changes in shape give rise to a need for an internal mechanism for accommodating deformation. In the case of plate martensite, where the final martensite may have a higher degree of tetragonality, that accommodation happens via internal twinning. Again, this is contrasted by lath

martensite, where the internal mode of deformation accommodation is slip (Pereloma and Edmonds, 2012). In both cases, these deformation modes are required to achieve the observed changes in both shape and orientation.

The first formal descriptions of the martensite transformation were given simultaneously by Wechsler et al. (1953) and Bowles and Mackenzie (1954). Both works describe the geometric constraints on the martensite transformation, and show how those constraints can be used to determine a unique solution for the habit plane and orientation relationship for plate martensite. Their work forms the foundation of the PTMC. The PTMC describes the martensite transformation as an invariantplane deformation; this must be the case for the habit plane, where the austenite-martensite interface is observed to be invariant at length scales much larger than the austenite unit cell parameter. At shorter length scales, the habit plane can be described as an array of coherency dislocations forming a glissile interface that moves as a martensite particle grows (Christian, 1975; Pereloma and Edmonds, 2012). In addition to leaving the habit plane undistorted and unrotated, the deformation must correctly change an FCC lattice to a BCC or BCT lattice. These requirements are met by coupling the Bain strain B with a rigidbody rotation **R** and a lattice-invariant deformation **L** to give the deformation gradient

$$\mathbf{F} = \mathbf{RBL},\tag{A.1}$$

where the Bain strain is defined as

$$\mathbf{B} = \begin{pmatrix} \eta_1 & 0 & 0 \\ 0 & \eta_1 & 0 \\ 0 & 0 & \eta_2 \end{pmatrix} \quad \eta_1 = \frac{\sqrt{2}a^M}{a^A}, \eta_2 = \frac{c^M}{a^A}. \tag{A.2}$$

The Bain strain contains the principal stretches η_1 and η_2 that must occur for an FCC lattice to form a BCC or BCT lattice (permute the positions of η_1 and η_2 for a total of 3 Bain variants). These stretches are functions of a^A , and both a^M , and c^{M} , the lattice parameters of austenite and martensite, respectively. The Bain strain describes the transformation from one lattice to the other by a contraction along one axis of the FCC unit cell, and a uniform expansion in the other two axes. The Bain strain alone, however, will not produce the orientation relationships observed for martensite in steel, nor does it leave any plane undistorted and unrotated. As noted above, the Bain strain must be coupled with both a lattice-invariant deformation L and a rigid-body rotation R. The lattice-invariant deformation (either slip or internal twinning) allows for the martensite particle to change shape without changing the base lattice. This coupling is sufficient to define a habit plane that is undistorted, but rotated from its original position. The inclusion of the rigidbody rotation brings the habit plane back into its original orientation, now undeformed. The deformation tensor can then take the form given in equation A.1, and is equivalent to the dyadic form given in equation 5.

Appendix A.2. Lath martensite

While the PTMC is well suited to the description of the deformation required for plate martensite, lath martensite presents

several challenges. Because slip is the internal mechanism by which lath martensite accommodates its own shape change, the lattice-invariant deformation L of equation A.1 must be expressed as a the activation of slip on a combination of rational slip systems at smaller length scales. Early attempts to determine a single slip system that would serve as a suitable lattice-invariant deformation failed to provide satisfactory solutions (Kelly, 1992; Pereloma and Edmonds, 2012). More recent studies on the crystallography of lath martensite included a second slip system, providing additional degrees of freedom for the lattice-invariant strain and allowing for a solution that predicts habit plane orientations closer to what is actually observed (Sandvik and Wayman, 1983a,b,c; Kelly, 1992, 2006; Morito et al., 2003, 2006). This double-shear form of the deformation tensor takes the form of equation A.3, with S_1 and S_2 representing the shear deformation caused by slip on two different slip systems. The deformation gradient can then be defined as

$$\mathbf{F} = \mathbf{RBS_2S_1}.\tag{A.3}$$

Various studies (Sandvik and Wayman, 1983c; Kelly, 1992) examine the possible choices of shear systems S_1 and S_2 . Multiple authors (Kelly, 1992; Morito et al., 2003) tabulate the shape deformations for each variant of martensite using lattice parameters that correspond to pure iron. These shape deformations agree with observed habit planes formed by lath martensite, as well as observed orientation relationships. These lattice parameters are $a^A = 0.36313 \ nm$ for austenite and $a^{M} = 0.28974 \, nm$ for BCC martensite. These define the choice of B described by equation A.2. The shear systems S_1 and S_2 and their respective magnitudes of shear, g_1 and g_2 , are: $S_1 = (101)[-101]\gamma$ or $(112)[-1-11]\alpha'$ with $g_1 = 0.26488$ and $S_2 = (1\ 0\ 0)[0\ 1\ -1]\gamma$ or $(1\ 1\ 0)[-1\ 1\ -1]\alpha'$ with $g_2 = 0.09122$. Ultimately, the double-shear system for the crystallography of lath martensite provides satisfactory predictions of habit plane orientations and orientation relationships.

References

Balluffi, R. W., Allen, S. M., Carter, W. C., and Kemper, R. A. (2005). *Kinetics of materials*. J. Wiley & Sons, Hoboken, N.J.

Beese, A. M. and Mohr, D. (2011). Effect of stress triaxiality and lode angle on the kinetics of strain-induced austenite-to-martensite transformation. *Acta Materialia*, 59(7):2589–2600.

Bowles, J. S. and Mackenzie, J. K. (1954). The crystallography of martensite transformations .1. *Acta Metallurgica*, 2(1):129–137.

Cantara, A. M., Zecevic, M., Eghtesad, A., Poulin, C. M., and Knezevic, M. (2019). Predicting elastic anisotropy of dual-phase steels based on crystal mechanics and microstructure. *International Journal of Mechanical Sci*ences, 151:639–649.

Caspersen, K. J. and Carter, E. A. (2005). Finding transition states for crystalline solid–solid phase transformations. *Proceedings of the National Academy of Sciences*, 102(19):6738–6743.

Chen, Y. and Schuh, C. A. (2015). A coupled kinetic monte carlo-finite element mesoscale model for thermoelastic martensitic phase transformations in shape memory alloys. *Acta Materialia*, 83:431–447.

Christian, J. W. (1975). The theory of transformations in metals and alloys: an advanced textbook in physical metallurgy. International series on materials science and technology v 15. Pergamon Press, Oxford; New York, 2d allition.

Cramer, J., Adams, D., Miles, M. P., Fullwood, D. T., Homer, E. R., Brown, T., Mishra, R. K., and Sachdev, A. (2018). Effect of strain path on forming

- limits and retained austenite transformation in q&p 1180 steel. Materials Science and Engineering a-Structural Materials Properties Microstructure and Processing, 734:192-199.
- De Moor, E., Lacroix, S., Clarke, A., Penning, J., and Speer, J. (2008). Effect of retained austenite stabilized via quench and partitioning on the strain hardening of martensitic steels. Metallurgical and Materials Transactions A. 39(11):2586.
- Ennis, B., Jimenez-Melero, E., Atzema, E., Krugla, M., Azeem, M., Rowley, D., Daisenberger, D., Hanlon, D., and Lee, P. (2017). Metastable austenite driven work-hardening behaviour in a trip-assisted dual phase steel. International Journal of Plasticity, 88:126–139. Gibbs, P. K. (2019). Strain Path Effect on Austenite Transformation and Duc-
- tility in TBF 1180 Steel. PhD thesis, Brigham Young University.
- Goodwin, G. M. (1968). Application of Strain Analysis to Sheet Metal Forming Problems in the Press Shop. SAE Transactions, 77:680093. 380-387
- Haidemenopoulos, G. N., Aravas, N., and Bellas, I. (2014). Kinetics of strain-induced transformation of dispersed austenite in low-alloy trip steels. Materials Science and Engineering a-Structural Materials Properties Microstructure and Processing, 615:416-423.
- Homer, E. R. and Schuh, C. A. (2009). Mesoscale modeling of amorphous metals by shear transformation zone dynamics. Acta Materialia, 57(9):2823-
- Hsu (Xu Zuyao), T. Y. (2006). Martensitic transformation under stress. Materials Science and Engineering: A, 438-440:64 - 68. Proceedings of the International Conference on Martensitic Transformations.
- Kalidindi, S. R., Bronkhorst, C. A., and Anand, L. (1992). Crystallographic texture evolution in bulk deformation processing of fcc metals. Journal of the Mechanics and Physics of Solids, 40(3):537-569.
- Kaufman, L. and Cohen, M. (1958). Thermodynamics and kinetics of marten-sitic transformations. *Progress in Metal Physics*, 7:165–246.
- Keeler, S. P. and Backhofen, W. A. (1964). Plastic instability and fracture in sheet stretched over rigid punches . ASM Trans Q, 56:25-48
- Kelly, P. M. (1992). Crystallography of lath martensite in steels. *Materials Transactions JIM*, 33(3):235–242.
- Kelly, P. M. (2006). Martensite crystallography the role of the shape strain Materials Science and Engineering a-Structural Materials Properties Microstructure and Processing, 438:43-47.
- Lebedev, A. A. and Kosarchuk, V. V. (2000). Influence of phase transformations on the mechanical properties of austenitic stainless steels. International Journal of Plasticity, 16(7-8):749-767.
- Mackenzie, J. K. and Bowles, J. S. (1954). The crystallography of martensite transformations .2. Acta Metallurgica, 2(1):138-147.
- Mansourinejad, M. and Ketabchi, M. (2017). Modification of olson-cohen model for predicting stress-state dependency of martensitic transformation. Materials Science and Technology, 33(16):1948-1954.
- Marketz, F. and Fischer, F. D. (1994). Micromechanical modeling of stressassisted martensitic-transformation. *Modelling and Simulation in Materials Science and Engineering*, 2(5):1017–1046.
- Matlock, D. K. and Speer, J. G. (2009). Third generation of AHSS: microstructure design concepts, pages 185-205. Springer.
- Miles, M. P. (2019). personal communication.
- Morito, S., Huang, X., Furuhara, T., Maki, T., and Hansen, N. (2006). The morphology and crystallography of lath martensite in alloy steels. Acta Materialia, 54(19):5323-5331.
- Morito, S., Tanaka, H., Konishi, R., Furuhara, T., and Maki, T. (2003). The morphology and crystallography of lath martensite in fe-c alloys. Acta Materialia, 51(6):1789-1799.
- Olson, G. and Cohen, M. (1975a). Thermoelastic behavior in martensitic transformations. Scripta Metallurgica, 9(11):1247-1254.
- Olson, G. and Cohen, M. (1982a). Dislocation structure of martensitic interfaces. In Unknown Host Publication Title, pages 1209-1213. Metallurgical Soc of AIME.
- Olson, G. and Cohen, M. (1986). Dislocation theory of martensitic transforma-
- tions. In *Dislocations in solids*, pages 295–407. North-Holland. Olson, G. B. and Azrin, M. (1978). Transformation behavior of trip steels. Metallurgical Transactions a-Physical Metallurgy and Materials Science, 9(5):713-721.
- Olson, G. B. and Cohen, M. (1975b). Kinetics of strain-induced martensitic
- nucleation. *Metallurgical Transactions*, A 6(4):791–795.
 Olson, G. B. and Cohen, M. (1982b). Stress-assisted isothermal martensitictransformation - application to trip steels. Metallurgical Transactions a-

- Physical Metallurgy and Materials Science, 13(11):1907-1914.
- Pati, S. R. and Cohen, M. (1969). Nucleation of the isothermal martensitic transformation. Acta Metallurgica, 17(3):189-199.
- Paul, S. K. (2013). Theoretical analysis of strain- and stress-based forming limit diagrams:. The Journal of Strain Analysis for Engineering Design, 48(3):177-188.
- Perdahcioğlu, E., Geijselaers, H. J., and Huetink, J. (2008). Influence of stress state and strain path on deformation induced martensitic transformations. Materials Science and Engineering: A, 481:727–731.
- Pereloma, E. and Edmonds, D. V. (2012). Phase transformations in steels. Woodhead Publishing in materials. Woodhead Publishing, Oxford ; Philadelphia.
- Sandvik, B. P. J. and Wayman, C. M. (1983a). Characteristics of lath martensite .1. crystallographic and substructural features. Metallurgical Transactions a-Physical Metallurgy and Materials Science, 14(5):809-822.
- Sandvik, B. P. J. and Wayman, C. M. (1983b). Characteristics of lath martensite .2. the martensite-austenite interface. Metallurgical Transactions a-Physical Metallurgy and Materials Science, 14(5):823-834.
- Sandvik, B. P. J. and Wayman, C. M. (1983c). Characteristics of lath martensite .3. some theoretical considerations. Metallurgical Transactions a-Physical Metallurgy and Materials Science, 14(5):835-844.
- Santacreu, P. O., Glez, J. C., Chinouilh, G., and Frohlich, T. (2006). Behaviour model of austenitic stainless steels for automotive structural parts. Steel Research International, 77(9-10):686-691.
- Seo, E. J., Cho, L., Estrin, Y., and De Cooman, B. C. (2016). Microstructuremechanical properties relationships for quenching and partitioning (q&p) processed steel. Acta Materialia, 113:124-139.
- Stringfellow, R. G., Parks, D. M., and Olson, G. B. (1992). A constitutive model for transformation plasticity accompanying strain-induced martensitic transformations in metastable austenitic steels. Acta Metallurgica Et Materialia,
- Taleb, L. and Sidoroff, F. (2003). A micromechanical modeling of the greenwood-johnson mechanism in transformation induced plasticity. International Journal of Plasticity, 19(10):1821-1842.
- Tjahjanto, D. D., Turteltaub, S., and Suiker, A. S. J. (2008). Crystallographically based model for transformation-induced plasticity in multiphase carbon steels. Continuum Mechanics and Thermodynamics, 19(7):399-422.
- Turteltaub, S. and Suiker, A. S. J. (2006). A multiscale thermomechanical model for cubic to tetragonal martensitic phase transformations. International Journal of Solids and Structures, 43(14-15):4509-4545
- Vasoya, M., Kondori, B., Benzerga, A. A., and Needleman, A. (2019). Energy dissipation rate and kinetic relations for Eshelby transformations. Journal of the Mechanics and Physics of Solids, page 103699.
- Voter, A. F. (2007). Introduction to the kinetic monte carlo method. In Sickafus, K. E., Kotomin, E. A., and Uberuaga, B. P., editors, Radiation Effects in Solids, pages 1-23, Dordrecht. Springer Netherlands.
- Wang, L. and Speer, J. G. (2013). Quenching and partitioning steel heat treatment, Metallography, Microstructure, and Analysis, 2(4):268-281.
- Wechsler, M. S., Lieberman, D. S., and Read, T. A. (1953). On the theory of the formation of martensite. Transactions of the American Institute of Mining and Metallurgical Engineers, 197(11):1503–1515.
- Yu, H. Y., Kai, G. Y., and De Jian, M. (2006). Transformation behavior of retained austenite under different deformation modes for low alloyed tripassisted steels. Materials Science and Engineering: A, 441(1-2):331-335
- Zecevic, M., Korkolis, Y. P., Kuwabara, T., and Knezevic, M. (2016). Dualphase steel sheets under cyclic tension-compression to large strains: Experiments and crystal plasticity modeling. Journal of the Mechanics and Physics of Solids, 96:65-87.
- Zecevic, M., Upadhyay, M. V., Polatidis, E., Panzner, T., Van Swygenhoven, H., and Knezevic, M. (2019). A crystallographic extension to the Olson-Cohen model for predicting strain path dependence of martensitic transformation. Acta Materialia, 166:386-401.

Conflict of Interest

Declaration of interests

☑ The authors declare that they have no known competing financial interests or personal relationships that could have appeared to influence the work reported in this paper.

☐ The authors declare the following financial interests/personal relationships which may be considered as potential competing interests:

Eric R. Homer Associate Professor

Department of Mechanical Engineering

Brigham Young University

Provo, UT 84602